Feasibility analysis of sea water flooding concept for marine-application LFR

Min Ho Lee, Il Soon Hwang, In Cheol Bang*
Department of Nuclear Engineering
Ulsan National Institute of Science and Technology (UNIST)
50 UNIST-gil, Ulju-gun, Ulsan 44919, Republic of Korea
**Corresponding author: icbang@unist.ac.kr*

1. Introduction

Nuclear energy has unique characteristics like high power density and long refueling frequency. Due to these characteristics, it has many advantages for energy system which is isolated from supply and high power is required, such as an icebreaker, an aircraft carrier, and an oil prospecting ship. In addition, many ships and submarines have been developed employing nuclear energy. Long refueling cycle, sufficient power, and silence are advantages of the nuclear-powered marine transportation.

In UNIST, to apply nuclear power to marine application, lead-bismuth eutectic (LBE)-cooled fast reactor (LFR) is under development, which is named as micro-URANUS. Because the micro-URANUS is focus on the marine application, robust and reliable decay heat removal system is required to guarantee coolability under extreme condition. The micro-URANUS adopted sea water flooding concept for one of the decay heat removal system, whose final heat sink is abundant sea water.

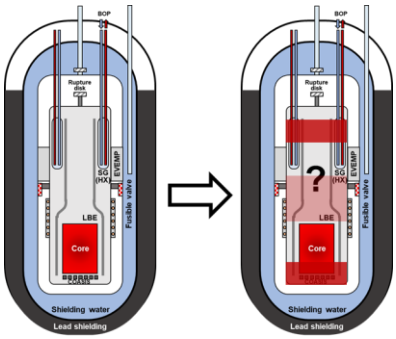

Fig. 1. Schematic of the micro-URANUS and relocation

LBE, which is coolant of micro-URANUS, has favorable characteristics for natural circulation, like high thermal conductivity and proper thermal expansion coefficient. Many reactors which are under development adopted natural circulation driven safety systems [1, 2]. Even pump-free reactor concept been considered by several groups [3-5]. Therefore, effective natural circulation and corresponding low peak temperature inside of the reactor vessel (RV) could be anticipated by LBE coolant during sea water flooding even after relocation.

The sea water flooding concept is very similar to in-vessel retention through external reactor vessel cooling (IVR-ERVC) of a pressurized water reactor (PWR). A main advantage of IVR-ERVC is guarantee of the integrity of the RV and prevention of the leakage of the radioactive materials. It is anticipated that similar advantages could be secured by the water flooding concept. In case of PWR, feasibility of the IVR-ERVC was evaluated based on two phenomena; one is ablation of the RV and failure of the RV, and the other is coolability at the external surface of the RV and margin for critical heat flux (CHF), which is a limit of coolability [6]. Similar methodology was adopted in this study for feasibility analysis of the water flooding for micro-URANUS.

To show feasibility of the water flooding concept under every situation, coolability of the water flooding concept was analyzed from extreme condition with overall melting of the RV inside. Configuration of the RV inside after relocation was reasonably assumed based on material properties. And based on the configurations, heat flux and temperature, which were related to main safety parameter for success of water flooding, would be discussed.

2. Numerical methodology

In this section, assumption for configuration inside of the RV after relocation, modeling of the heat transfer system, and a numerical procedure for solving established model were described.

2.1 Assumption for configuration of relocated corium

Inside of the RV, there are three kinds of materials: fuel, structural metal, and LBE coolant. After melting, they were relocated according to their properties, especially density. However, they could be mixed depending on their density and compatibility. LBE coolant and structural metal are metal in common. And density of the LBE and oxide fuel is quite similar. Based on these, configuration of the relocated corium was assumed like figure 2.

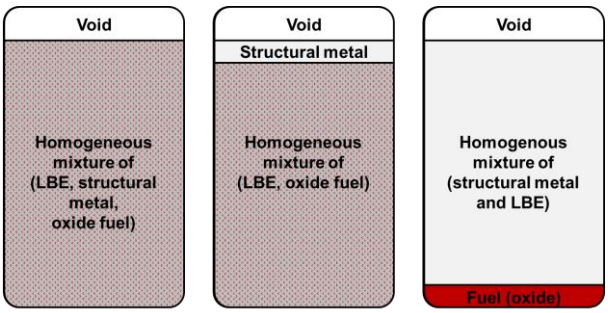

(a) all mixed (b) 2-layer w. met. (c) 2-layer w. ox.

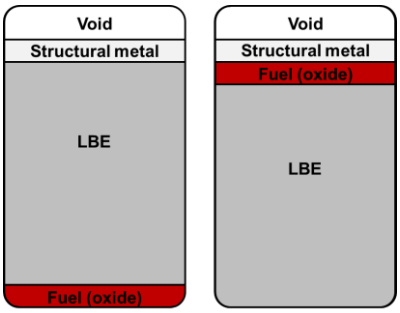

(d) 3-layer ox. immersed (e) 3-layer ox. floated
Fig. 2. Configuration of relocated corium

It was assumed that there is void on the top of the corium to be more conservative in terms of CHF limit for cooling. It would be discussed in more detail in the following section. Case (a) is the simplest case, where whole materials were mixed homogeneously. Case (b) and (c) are two-layer model. In the aspect of the density, LBE and oxide fuel are very similar, thus, they could be mixed and formed new layer as mixture of LBE and oxide fuel, like (b). However, in the aspect of material compatibility, LBE and structural metal could be mixed because there are metal in common, like (c). Mixture of structural metal and oxide fuel was not considered because they were not mixed, and it was validated through experiments with real material [7, 8]. Case (d) and (e) are three-layer model, where the LBE, oxide fuel and structural metal were separated from each other. Difference between (d) and (e) is position of the oxide fuel. Both situations could happen because density of the LBE and oxide fuel are quite similar.

2.2 Heat transfer modeling

Heat transfer in the system was simplified as 1-D lumped capacitance method, which was already adopted in the PWR analysis [6]. Considering heat transfer under water flooding, heat was only generated in the layer including oxide fuel. This heat could be removed by several ways. First one is lateral heat transfer, which has the shortest thermal circuit in this system. Here, natural circulation inside layer including fuel, conduction through the RV wall, and boiling heat transfer at the external surface of the RV wall should be considered. Regard to the upward and downward heat transfer, natural circulation inside in the layer including fuel, natural circulation or conduction inside of adjacent layer, conduction through the RV wall, and boiling heat transfer at the external surface of the RV wall should be considered. To be more conservative, radiation heat transfer to the void side was neglected.

They were summarized in equations below with case (d) as an example. Heat was only removed by boiling at the external surface of the RV.

$$Q_{total} = Q_{bot} + Q_{top} + Q_{lateral}$$

$$\begin{aligned} Q_{bot,fuel} &= h_{fuel} A_{bot} \left(T_{fuel,bulk} - T_{RV,fuel,bot,in} \right) \\ &= \left(k_w / d_w \right) A_{bot} \left(T_{RV,fuel,bot,in} - T_{RV,fuel,bot,out} \right) \\ &= C_{boil} A_{bot} \left(T_{RV,fuel,bot,out} - T_{sat} \right) \end{aligned}$$

$$\begin{aligned} Q_{top,fuel} &= h_{fuel} A_{top} \left(T_{fuel,bulk} - T_{int,fuel-LBE} \right) \\ &= Q_{LBE,top} + Q_{LBE,lateral} \end{aligned}$$

$$\begin{aligned} Q_{LBE,lat} &= h_{fuel} A_{LBE,lat} \left(T_{LBE,bulk} - T_{RV,LBE,in} \right) \\ &= \left(k_w / d_w \right) A_{LBE,lat} \left(T_{RV,LBE,in} - T_{RV,LBE,out} \right) \\ &= C_{boil} A_{LBE,lat} \left(T_{RV,LBE,out} - T_{sast} \right) \end{aligned}$$

$$\begin{aligned} Q_{LBE,top} &= Q_{metal,bot} \\ &= Q_{metal,side} \\ &= h_{LBE,top} A_{top} \left(T_{LBE,bulk} - T_{int,LBE-metal} \right) \\ &= h_{metal,bot} A_{bot} \left(T_{int,LBE-metal} - T_{metal,bulk} \right) \\ &= h_{metal,lat} A_{metal,lat} \left(T_{metal,bulk} - T_{RV,metal,in} \right) \\ &= \left(k_w / d_w \right) A_{metal,lat} \left(T_{RV,metal,in} - T_{RV,metal,out} \right) \\ &= C_{boil} A_{metal,lat} \left(T_{RV,metal,out} - T_{sat} \right) \end{aligned}$$

$$C_{boil} = \left[\frac{g \left(\rho_L - \rho_V \right)}{\sigma_L} \right]^{1/2} \left(\frac{c_{p,L}}{h_{fg} C_{sf} Pr_L} \right)^3 \left(\mu_L h_{fg} \right)$$

Overall heat balance of the system was summarized, and boiling was modeled as Rohsenow correlation using constant C_{boil}.

Global Nusselt numbers were calculated based on the proper correlations, while local Nusselt number was calculated based on the laminar assumption, like equation below.

$$Nu_{local} = \frac{4}{3} \overline{Nu} \times \left(\frac{z}{H} \right)^{\frac{3}{4}}$$

It was applied to the layer which has larger thickness to diameter ratio than 1/3 or has large Prandtl number like oxide layer.

2.3 Numerical procedure

Overall heat balance and bulk temperature could be calculated using equations in the previous section. However, heat transfer coefficient h is a function of temperature. It means that the heat transfer coefficient

is affected by temperature, which is calculated based on the heat transfer coefficient. To obtain final temperature and corresponding heat transfer coefficient, iterative method was used by updating temperature and heat transfer coefficient alternatively. If temperature did not change more than criterion, that temperature was treated as solution.

Next step is obtaining local distribution of the heat flux in each layer. According to previous criteria like thickness to diameter ratio and Prandtl number, vertical variation of the parameter was calculated for all kind of mixture, oxide layer, and LBE layer. The structural metal layer was excluded, and vertical variation of the parameter was neglected. Vertical variation of the local parameter could be calculated based on the bulk parameter. Regard to calculation of the vertical variation, Newton-Raphson method were used for multiple variables.

3. Results and Discussion

In so far, case (a) and (b) were analyzed and the other cases are under analyzing. Therefore, case (a) and (b) could be discussed in this session, and other cases would be updated. All cases were compared at 2% of the decay heat, and for the most severe case, CHF limit would be compared with heat flux at the external surface and corresponding decay power.

If temperature of a layer is lower than melting temperature of the layer, it was assumed as solid and conduction equation was adopted instead of convection equation. If a layer is mixture, melting temperature of the mixture was assumed as that of the LBE and other components were suspended in the LBE.

In the aspect of maximum temperature of the corium, case (a) is the best case because heat source is distributed evenly in the LBE coolant and structural metal chunk, which have high thermal conductivity. It is similar to case (b), because fuel was suspended in the LBE coolant. However, in case of oxide layer separation, like case (c), (d), and (e), temperature increase of the increase is inevitable because thermal conductivity of the molten oxide fuel is low. In addition, there is probability of formation of crust of the oxide, which is solidification oxide due to low temperature. It could reduce molten volume of the oxide layer and degrade natural circulation inside of the oxide layer, which cause further increase of the maximum temperature.

Regard to the heat flux and corresponding CHF margin, thickness of the highly conductive layer is important [6]. Similar to the maximum temperature, case (a) and (b) is less severe than other cases because heat could be well dispersed by the LBE. Since heat was transferred more to upward than downward under natural circulation, case (e) is expected to have the highest focused heat flux and the smallest safety margin for CHF, coolability.

First, maximum temperature inside of layer including fuel is approximately 228°C in case (a) and 272°C in case (b). Here, melting temperature of the oxide fuel, structural metal, and LBE is approximately 2700°C, 1300°C and 124°C, respectively. Considering these melting temperatures, to be assumed as case (a) solidified oxide fuel and structural metal were suspended in the molten LBE. It is similar to the case (b), and solidified oxide fuel is suspended in the LBE layer with separated solid structural metal layer.

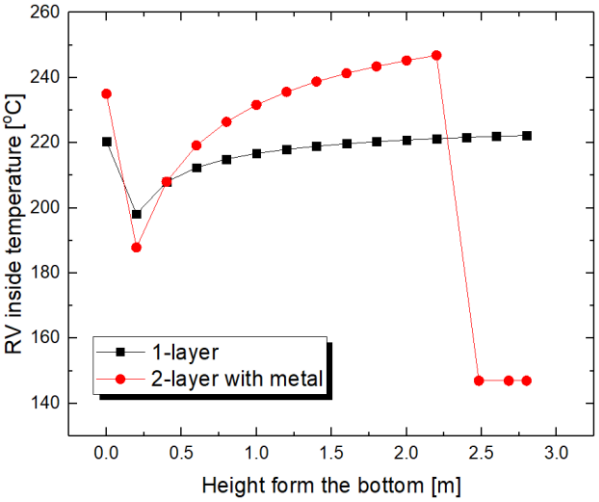

Fig. 3. Temperature inside of the reactor vessel

Figure 3 shows the temperature inside of the reactor vessel. Bulk temperature of the structural metal in case (b) was calculated as 240°C, which was much lower than melting temperature of approximately 1300°C. Therefore, the structural metal layer was treated as solid and conduction mode applied.

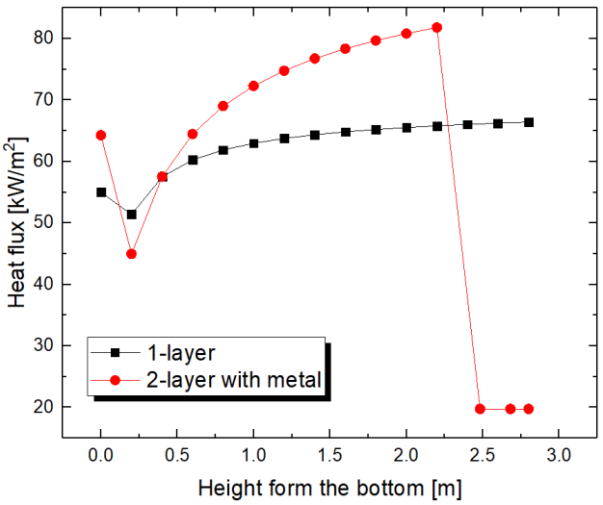

Fig. 4. Heat flux with different vertical position

1-layer model showed increased temperature as vertical position goes upward. It is caused by local variation of the Nusselt number; higher position has higher local Nusselt number. In case of 2-layer model with separated structural metal layer, slightly higher

temperature was expected because of increase of thermal resistance at the solid metal layer part. Thermal resistance of the structural metal layer is higher than that of the mixture of fuel and LBE, thus, heat was mainly removed by the lateral surface of the mixed layer. Melting temperature of the RV is about 1300°C, therefore, it could be concluded that under 2% of the decay heat level, there is no concern for RV failure by melting.

It could be more easily recognized by heat removal by the boiling at the external surface of the RV. Boiling could make significant difference of the heat flux level by small temperature difference. Because boiling condition was given to the external surface of the RV, temperature at the external surface was almost similar. Therefore, tendency of the graph is very similar to figure 3. Only 4 % of the heat was removed through the solidified structural metal layer, so heat flux at the metal layer was significantly lower. The maximum heat flux was anticipated as 81.8 kW/m^2, which is much lower than typical CHF limit as 1000 kW/m^2. From these values, water flooding concept could remove 2 % decay heat without concern about CHF.

Considering analysis results, under 2% of decay heat, feasibility of the water flooding concept was validated with case (a) and (b).

4. Conclusions & Further works

To evaluate applicability of the water flooding concept of the micro-Uranus, temperature and heat flux distribution was calculated by 1-D lumped capacitance method.

Currently, 2% of the decay heat was assumed and relocation of the core material was assumed as case (a) and (b). Under given condition, both cases did not show melting of the RV or threatening of the CHF limit. Both temperature and heat flux were far below the safety criterion. Therefore, water flooding concept could be successful for micro-Uranus under given condition.

For the further work, analysis of the other cases (case (c), (d), and (e) would be conducted. Regard to the most severe case, effect of decay heat on the temperature and CHF margin would be evaluated by parametric study.

ACKNOWLEDGEMENT

This work was supported by the Nuclear Energy Research Program through the National Research Foundation of Korea (NRF) funded by the Korea government (MSIT) (2020M2A8A4022882, NRF-2019M2D1A1067205).

REFERENCES

[1] A. Alemberti, V. Smirnov, C. F. Smith, and M. Takahashi, Overview of Lead cooled Fast Reactor Activities, Progress in Nuclear Energy, Vol.77, p.300, 2014.
[2] A. Alemberti, M. L. Frogheri, S. Hermsmeyer, L. Ammirabile V. Smirnov, M. Takahashi, C. F. Smith, Y. Wu, and I. S. Hwang, Lead cooled Fast Reactor (LFR) Risk and Safety Assessment White Paper, Gen IV International Forum 2014.
[3] C, F, Smith, W. G. Halsey, N. W. Brown, J. J. Sienicki, A. Moisseytsev, and D. C. Wade, SSTAR: The US lead-cooled fast reactor (LFR), Journal of nuclear materials, Vol.376, p.255, 2008.
[4] M. Takahashi, S. Uchida, and Y. Kasahara, Design Study on reactor structure of Pbi-Bi-cooled direct contact boiling water fast reactor (PBWFR), Progress in Nuclear Energy, Vol.50, p.197, 2008.
[5] J. Buongiorno and N. E. Todreas, Conceptual design of a lead-bismuth cooled fast reactor with in-vessel direct-contact steam generation, MIT-ANP-TR-079, Massachusetts Institute of Technology, 2001.
[6] Y. J. Cho, H. S. Park, M. H. Choi, S. W. Hwang, and H. K. Noh, Development of Assessment Methodologies for Corium Coolability, KINS/HR-1410, 2015.
[7] V. Asmolov, Latest findings of RASPLAV project, No. NEA-CSNI-R--1998-18. 1999.
[8] V. Asmolov, and D. Tsurikov, MASCA project: major activities and results, CSNI Workshop, MASCA Seminar, 2004.